# DESIGN OF WIND TUNNEL RIG FOR THE TEST OF A SINGLE ELECTRICAL LIFT THRUST UNIT DURING CONVERSION MANEUVER


**Giacomo Lazzaro**
Politecnico di Milano
Milano, Italy

**Stefano Bedin**
Leonardo Helicopters
Samarate, Italy

**Antonio Tomaselli**
Politecnico di Milano
Milano, Italy

**Federico Pellegrino**
Leonardo Helicopters
Samarate, Italy

**Vincenzo Muscarello**
RMIT University
Melbourne, VIC, Australia

**Pierangelo Masarati**
Politecnico di Milano
Milano, Italy

**Michele Zilletti**
Leonardo Helicopters
Samarate, Italy



## ABSTRACT

The aeronautical community is increasingly focusing on innovative multi-propeller electric Vertical Take-Off and Landing aircraft for Advanced Air Mobility. This paper presents the development and validation of methodologies and tools to support the early-stage design of such aircraft. In particular, it focuses on the design of an experimental wind tunnel test rig featuring an electric Lift-Thrust Unit (eLTU) equipped with a tilting mechanism that enables smooth transition between helicopter (H/C) mode and airplane (A/P) mode and independent control of the rotor speed. The test rig integrates a load cell and strain gauges to measure the loads generated by the eLTU under various flight conditions, as well as encoders to track the motion of the tilting mechanism. A numerical aeroelastic model has been developed to guide the rig design and to analyze the coupled aerodynamic and structural behavior of the eLTU and tilting system. Preliminary correlation results from tests conducted without wind are presented, demonstrating the robustness and reliability of the experimental setup in preparation for future wind tunnel campaigns.


## INTRODUCTION

The integration of electric propulsion systems into rotary-wing aircraft has broadened the possibilities for innovative vehicle architectures. These novel designs offer several potential benefits, including improved safety through propulsion system redundancy, zero emissions with fully electric power, and a simplified drive system that could lower production and maintenance costs while improving overall reliability. As highlighted in recent literature (Refs. 1, 2), despite the diversity of these novel air vehicle architectures, they share common features such as multiple LTUs, tilting capability, and variable RPM for thrust control. Notable examples of aircraft exploiting these features include the *S4* by Joby Aviation and the *Aero3* by Dufour Aerospace, the latter featuring a tiltwing configuration equipped with multiple rotors.

In recent years, increasing attention has been given to the impact of these features on the aeroelastic response of LTUs and the resulting load generation mechanisms. For instance, Zilletti et al. (Refs. 3, 4) designed and tested a setup to characterize the static and dynamic load generation mechanisms of one (Ref. 3) and two (Ref. 4) electrical LTUs mounted on a common structure. Their findings revealed that a stiff rotor could generate significant oscillatory loads over a broad frequency range, with magnitudes comparable to the corresponding static loads, particularly in edgewise airflow conditions. Building on this research, this paper focuses on the prediction of the loads of the same LTU of (Ref. 3) equipped with an actuated tilting mechanism in different wind conditions.

In the development of tilting lift-thrust units (LTUs), a range of architectures adopted by leading manufacturers has been reviewed to evaluate their respective advantages and limitations. Two distinct design philosophies have emerged from this analysis. The first involves mechanically complex systems aimed at optimizing LTU conversion while simultaneously addressing other design objectives, such as minimizing aerodynamic blockage by optimizing the rotor disk with respect to the wing (Ref. 5). The second approach emphasizes simplicity, favoring more compact and simpler mechanical solutions (Ref. 6). While the former can accommodate multiple performance requirements, the latter offers clear benefits in terms of mechanical simplicity, scalability, and manufacturability. In line with the study's objectives of compactness, manufacturing simplicity, and minimal mechanical complexity, a simplified four-bar linkage mechanism was chosen.

In electrically powered aircraft, tilting mechanisms are typically actuated using electromechanical actuators (EMAs). These actuators are inherently rotational, as they are generally driven by rotary electric motors. In linear EMAs, this rotational motion is converted into linear displacement through mechanisms such as roller-screw assemblies. Although linear actuators offer benefits, such as high linear force output, precise position control, and inherent self-locking capabilities, a rotary EMA was chosen for this study. This selection aligns with previously defined design requirements of scalability, compactness, and reduced mechanical complexity characteristics, commonly associated with rotary actuation systems.

## TEST RIG DESIGN

### Tilting mechanism optimization

A multibody model of the LTU system has been developed to investigate how different arrangements of the selected kinematic architecture affect the actuator sizing requirements, particularly in terms of actuation torque. As shown in Figure 1, the multibody model consists of a set of rigid bodies (depicted in gray) representing the different elements of the system:

1. Propeller;
2. Motor-load cell assembly;
3. Tilting plate;
4. Rod;
5. Actuator.

The red parts denote the components anchored to the ground. The rigid bodies are connected by means of hinges as schematically shown in Figure 1 by the blue dots (A,B,C,D). A control moment is applied at hinge C to simulate the actuation, while rotation is measured at hinges C and D to monitor the mechanism's motion. Due to the symmetry of the system, the motion of the model is constrained within the XZ-plane.

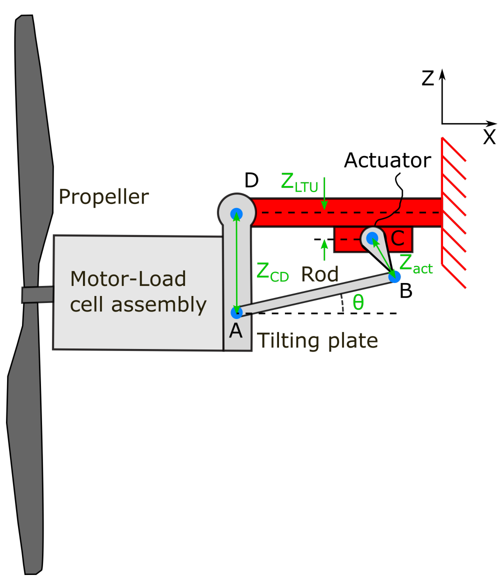


**Figure 1. Mechanism architecture.**

The green geometrical parameters highlighted in the schematic represent the key design variables considered during the design process. The overall design workflow, illustrated in Figure 2, can be divided into four main steps:

**Step 1** - Generation of design space:
The key design parameters are selected as the primary design variables. A set of feasible mechanism configurations is identified, ensuring compliance with the maximum allowable overall dimensions of the system.

**Step 2** - Mechanism feasibility:
Each configuration is evaluated to verify its geometric feasibility.

**Step 3** - Unitary load simulation:
For each configuration deemed feasible, an initial simulation is performed in which the actuator is driven with a prescribed rotational input, while a unitary torque load is applied at the LTU hinge point D. The objective of this simulation is to evaluate the configuration's mechanical advantage (MA), as defined in Equation 1.

$$MA = \frac{M_o}{M_i} = \frac{\omega_i}{\omega_o} \tag{1}$$

The simulation runs until either the maximum simulation time is reached or the LTU completes its full transition. A configuration is considered a valid candidate for the final design step if the mechanical advantage remains above a predefined threshold throughout the motion and the target end position is successfully achieved.

**Step 4** - Actuator sizing:
The final step consists of a dynamic simulation in which a prescribed motion is applied to the actuator, this time under a complete set of LTU loads representative of the most demanding wind tunnel conditions. These loads are obtained from post-processed data collected during the wind tunnel test campaign described in (Ref. 3), and are expressed as functions of the LTU tilting angle. To capture the full dynamics of the system, the rotor disk is modeled to spin at its nominal rotational speed, thereby accounting for inertial effects. Gravitational forces are also included in the model. The peak actuator load observed during the simulation is recorded and used for comparative evaluation across all candidate configurations.

At the end of the design process, the configuration that minimizes the actuator torque requirement is selected. Its robustness to small variations in the design parameters, such as those that may arise during manufacturing and assembly, has been evaluated. A final verification of the mechanism and the encoders installation has been carried out on a 3D printed model. The results of the simulations have also led to the selection of an off-the-shelf actuator matching the torque requirement.

### Test rig description

The experimental rig developed for this study is based on the design parameters obtained from the design process described in the previous section. Figure 3 shows the LTU mounted on a six-axis load cell supported by the four-bar linkage mechanism actuated by the tilting actuator.

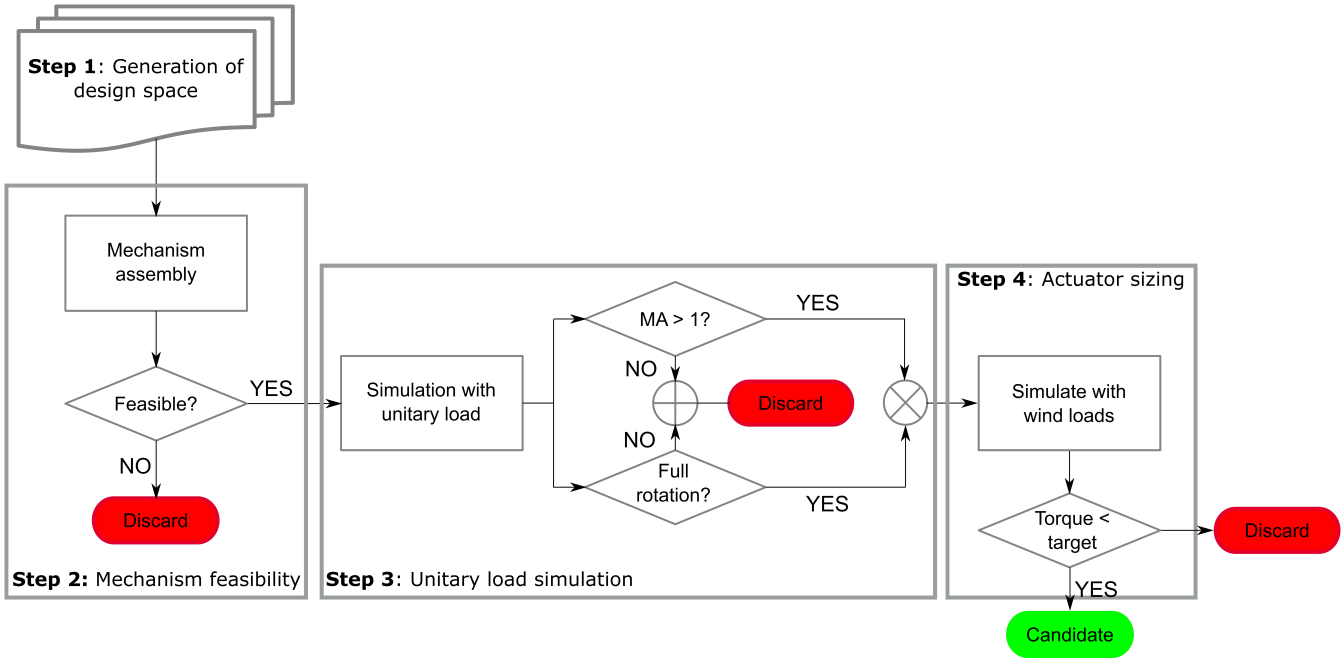


**Figure 2. Mechanism optimization workflow.**

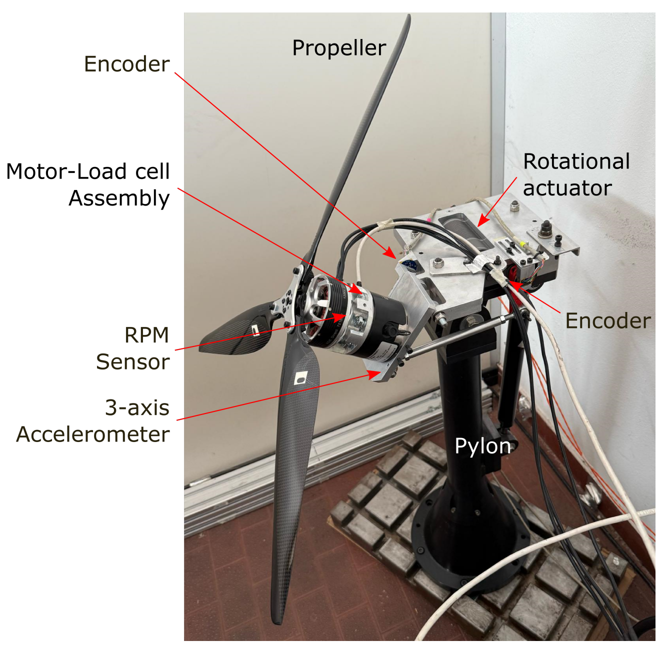


**Figure 3. Wind Tunnel Test Rig.**

The test rig is equipped with three 12-bit absolute encoders, used to measure the following parameters:

1. The angular velocity of the propeller, obtained by differentiating the angular position measured via $I^2C$ communication.
2. The tilting angle of the LTU, $\alpha$ (measured via analog signal).
3. The actuator angle, $\beta$ (measured via analog signal).

One method for estimating actuator torque is to measure the current drawn and multiply it by the actuator's torque constant. However, due to the high gear reduction ratio of the actuator (187:1), the torque required at the motor shaft is relatively low, resulting in minimal current draw. This makes the current measurement unreliable for accurately determining the output torque. Therefore, a half-bridge strain gauge has been installed on the rod connecting the actuator's servo arm to the tilting plate to directly measure the axial force, which can be used to infer the torque delivered by the actuator.

The communication between the control electronics and the tilting actuator is established via the UART protocol. To prioritize real-time performance, only essential parameters required for the motor control are transmitted, while non-critical telemetry data is minimized or omitted. The control system is implemented using two dedicated STM32 microcontrollers, with one assigned to the LTU motor control and the other to the tilting actuator. Custom PCBs have been developed to enhance system robustness and reliability.

The LTU motor is controlled using a closed-loop Proportional-Integral (PI) speed controller, with feedback derived from the propeller's angular position measured by an absolute encoder. The controller output generates a PWM signal, which is transmitted to the Electronic Speed Controller (ESC) via a dedicated channel. The reference speed is set by a separate control board based on an Arduino, equipped with an LCD interface. This setup enables remote operation of the test rig, allowing the reference signal to be adjusted from a dedicated control room. The same control architecture is applied to the tilting actuator. In this case, the reference position is also provided by an external

Arduino board, while the STM32 microcontroller initiates a proportional position control loop integrated within the actuator. Communication with the actuator is handled via the RS485 protocol, with command frames transmitted using the STM32's UART interface through a dedicated transceiver module. Motion profiles are executed by sending a sequence of reference positions to the actuator at fixed time intervals. This approach enables the actuator to follow a predefined motion trajectory within a set time window. As a result, the proportional gain of the controller must be carefully tuned: it must be high enough to ensure sufficient bandwidth for tracking the trajectory within the required timing constraints, yet low enough to avoid excessive responsiveness that could lead to irregular motion or repeated stopping.

## NUMERICAL MODEL

### LTU numerical model

The blade structure was modeled using MBDyn, a general-purpose multibody dynamics analysis software (Ref. 7), and validated against data available from previous work (Ref. 3). The blade is modeled using six elastic beam elements (*beam3* in MBDyn) positioned along its elastic axis, complemented by twelve lumped masses that replicate the mass and inertial properties of each corresponding blade section.

The *axial rotation* joint is added to constrain the mast rotating node with the fixed grounded node and to impose the angular velocity for the propeller rotation; the mast is then connected to the hub rotating node through linear and torsional springs (*deformable displacement joint* and *deformable hinge* in MBDyn) to correctly represent the elastic properties of the mast. Each blade is connected to the hub via a six-degree-of-freedom linear spring and a cantilevered flexible beam (*beam2* element in MBDyn) rigidly constrained at the hub. The stiffness properties of these elements have been tuned to match the eigenmodes of the propeller.

The MBDyn structural model was validated against the GyroX3 model and the experimental data reported in (Ref. 3). Table 1 compares the first three in-vacuum eigenfrequencies of the propeller at zero RPM, showing excellent agreement.

The blade aerodynamics were initially modeled in MBDyn using the strip theory module embedded in the multibody code, which enables the assignment of aerodynamic elements to each structural beam. To achieve higher fidelity, an aerodynamic model of the propeller was subsequently developed in DUST—an aerodynamic vortex particle solver (Ref. 8)—using 23 lifting-line elements. The DUST aerodynamic model is shown in Figure 4.

Figure 5 shows the validation results for static torque and thrust against the propeller RPM for a wind speed of 16 m/s and 40 degrees tilt angle (all data were non-dimensionalized using the maximum angular velocity tested, along with the highest aerodynamic thrust and torque measured during the experimental campaign from (Ref. 3)). Overall, all tools show good agreement with the experimental data for static load predictions.

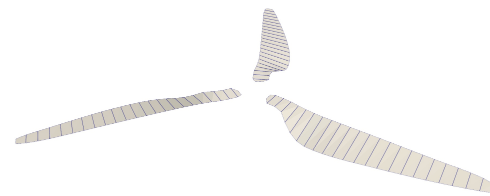

**Figure 4. DUST model of the propeller.**

The latter aeroelastic model has been obtained by integrating the structural MBDyn and aerodynamic DUST models using the open-source coupling tool PreCICE (Ref. 9). This framework ensures a tight coupling scheme, enabling continuous data exchange between the two solvers during the simulation, as described in (Ref. 10). The coupled MBDyn–DUST model is expected to be essential for capturing the aeroelastic dynamic loads, as these arise from the complex interaction between the structural dynamic response and the aerodynamic forces on the propeller.

### Tilting mechanism model

Initially, the mechanism was considered rigid and consequently modeled using ideal joints. Specifically, the input shaft was anchored to the ground through clamped joints, which defined the fixed reference frame. Rotation was introduced via an axial rotation joint about the vertical axis, driven by the analytical solution of the four-bar linkage. The resulting motion was transmitted to the mechanism through a series of revolute and total joints, representing the kinematics of the four-bar system. The total joints constrain two degrees of freedom while allowing rotation about a single axis.

To model the load cell's compliance, a deformable displacement joint was included. Its stiffness in the $z$-direction was calibrated to match the first natural frequency of the load cell, yielding a stiffness value of $k = 1.48 \times 10^7$ N/m.

Together, these elements reproduce the behavior of a classical four-bar linkage whose input rotation is converted into a controlled output rotation delivered to the tilting plate. Moreover, to correctly model the inertia of the experimental setup, the masses of all other system components are included in addition to the blades: the hub mass, the engine, the supporting structures and the six-component balance. Based on the geometry of the tilting mechanism, the kinematic relationship between the actuator angle $\beta$ and the tilt angle $\alpha$ was derived. The analytical relationship was then used to determine the actuator's velocity profile required to achieve a constant tilt rate of $\dot{\alpha} = 3°$/s.

## RESULTS

### Tilting Mechanis model correletion

First, the relationship between the actuator angle $\beta$ and the LTU tilting angle $\alpha$ is examined. Figure 6 compares the experimental, simulated, and analytical tilting angles as functions of the actuator angle, demonstrating excellent agreement.

| Description | GyroX3 [Hz] | MBDyn [Hz] | Error [%] |
|---|---|---|---|
| $1^{st}$ Bending out-of-plane | 59.3 | 58.6 | -1.20 |
| $1^{st}$ Bending in-plane | 216.9 | 219.4 | +1.15 |
| $2^{nd}$ Bending out-of-plane | 295.7 | 294.4 | -0.40 |

**Table 1. Comparison of eigen frequencies in vacuum at Ω = 0 RPM.**

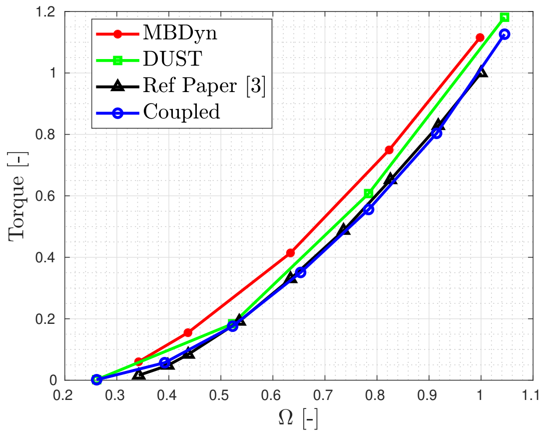


(a) Torque: $V_\infty = 16$ m/s, $\alpha = 40°$

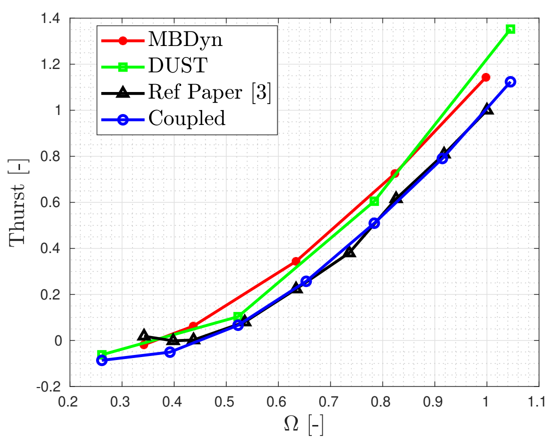


(b) Thrust: $V_\infty = 16$ m/s, $\alpha = 40°$

**Figure 5. Aerodynamic validation of the different models with experimental results.**

The mechanical advantage, defined in Equation 1 with $\omega_i = \dot{\beta}$ and $\omega_o = \dot{\alpha}$, is computed to further validate the correlation between experimental and simulated models. The angular speeds of the experimental data are obtained via numerical differentiation followed by filtering. Figure 7 illustrates the resulting MA values obtained from the experimental data and MBDyn.

Except for the initial phase, where the mechanical advantage falls below 1, the mechanism consistently requires a lower actuator moment than the resisting moment throughout the conversion maneuver, confirming its efficiency.

Following mechanism validation, the full test rig was assessed during the conversion maneuver. Direct actuator torque measurement was not feasible, as already mentioned; instead,

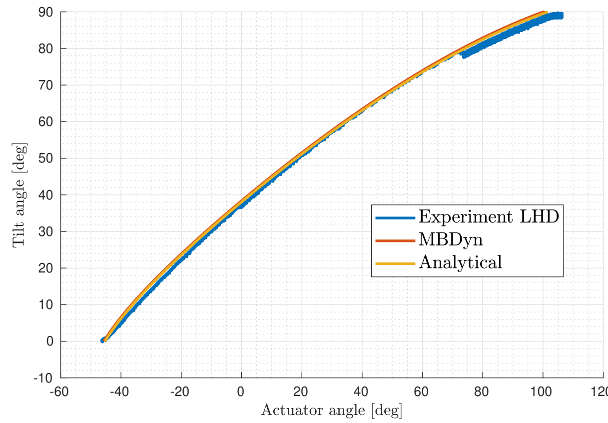


**Figure 6. Kinematics of the tilting mechanism.**

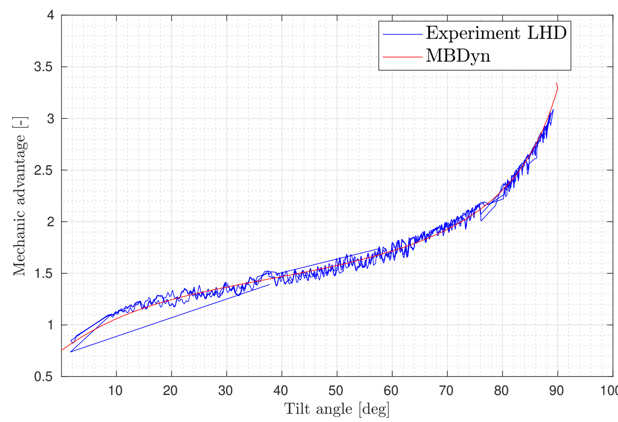


**Figure 7. Tilting mechanical advantage.**

the four-bar mechanism's rod was instrumented with a half-bridge strain gauge to capture axial force, enabling indirect validation of the actuator torque. The initial validation was performed in hover ($V_\infty = 0$ m/s) at $\Omega = 42\%$ RPM over a complete H/C–A/P–H/C conversion. Figure 8 compares the measured axial force with the MBDyn numerical simulations, with negative values indicating compression. The axial force is well captured during conversion. Notably, the experimental results exhibit a hysteresis effect, likely due to propeller wake ingestion during the H/C-A/P conversion maneuver, which modifies aerodynamic loading and thus the axial force on the rod. To verify this hypothesis, coupled MBDyn–DUST simulations—accounting for unsteady wake and interactional aerodynamics—are currently underway.

Another tested condition in hover ($V_\infty = 0$ m/s) at full rotational speed ($\Omega = 100\%$ RPM) is shown in Fig. 9. Again, the results show strong agreement. In this condition, the mean axial force is lower than in the previous case and reaches zero

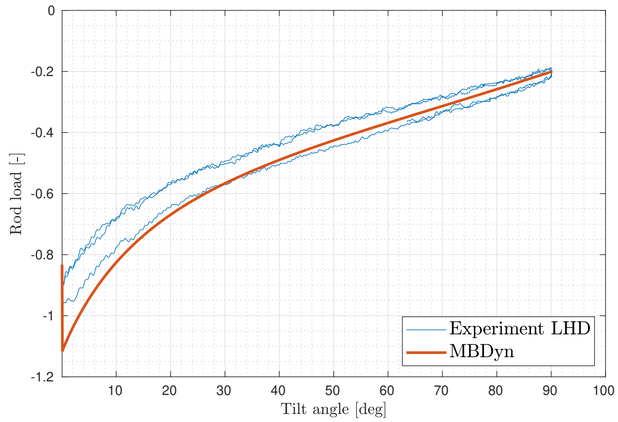


**Figure 8. Axial force for $V_\infty$ = 0 m/s and $\Omega$ = 42% RPM, during a conversion - reconversion maneuver.**

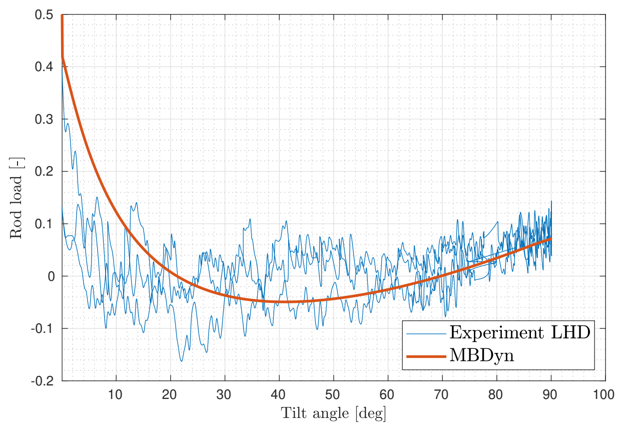


**Figure 9. Axial force for $V_\infty$ = 0 m/s $\Omega$ = 100% RPM.**

at two tilt angles, indicating that specific combinations of tilt angle and propeller RPM require little to no actuator effort. This load equilibrium—when static aerodynamic forces from the LTU balance the weight—may trigger freeplay nonlinearities and Limit Cycle Oscillations, potentially explaining the high-frequency oscillations observed in Fig. 9.

Finally, the control torque is reconstructed through the rod axial loads obtained from the MBDyn simulation models. Figure 10 shows the actuator torque for the latter aerodynamic condition. As expected, when the rod force reaches zero, the corresponding torque also crosses the x-axis. The increasing amplitude of the force oscillations further confirms that the simultaneous zero-force and zero-torque condition can trigger small imperfections within the mechanism.

### Preliminary loads correlation

Finally, the propeller aerodynamic loads in hover were measured using the load cell and compared with the simulated forces and moments from MBDyn and DUST. The force in the z-direction corresponds to propeller thrust, while the x- and y-components represent in-plane forces. Because the propeller, engine, and part of the supporting structure are mounted on the load cell and tilt with the assembly, their gravitational forces are included in the measurements. To isolate

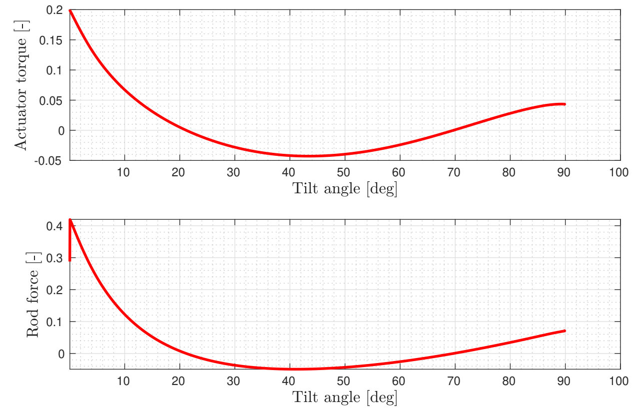


**Figure 10. Control torque for $V_\infty$ = 0 m/s $\Omega$ = 100% RPM obtained in MBDyn.**

the aerodynamic thrust, the gravity component—whose projection varies during the conversion maneuver—was removed during post-processing. This component was obtained from a conversion maneuver at $\Omega = 0$ RPM using the loads measured along the z-axis. Figure 11 shows the non-dimensional thrust and torque at $\Omega = 42\%$ RPM, compared with predictions from MBDyn and DUST.

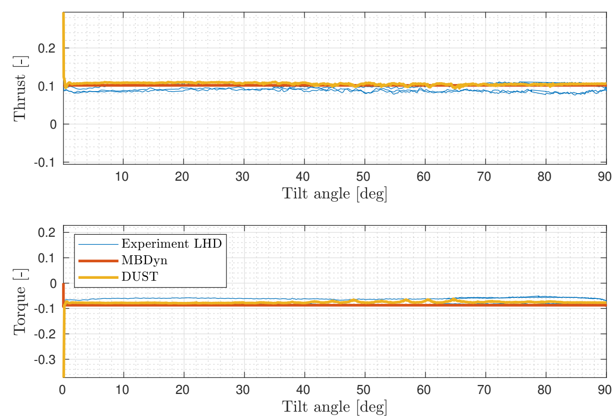


**Figure 11. Thrust and torque for $V_\infty$ = 0 m/s and $\Omega$ = 42% RPM.**

With null freestream velocity, the aerodynamic loads are constant through the entire conversion maneuver, as expected. For completeness, the corresponding plot at $\Omega = 100\%$ RPM is shown in Figure 12.

## CONCLUSIONS

1. The experimental setup, equipped with all necessary sensors and instruments, has been thoroughly tested, and the results show a strong correlation with numerical model simulations. This agreement confirms both the reliability of the sensors and the ability of the numerical model to accurately represent the physical behavior of the system. The force measured in the connecting rod has been used for correlation purposes, allowing the numerical actuator torque to be considered reliable.

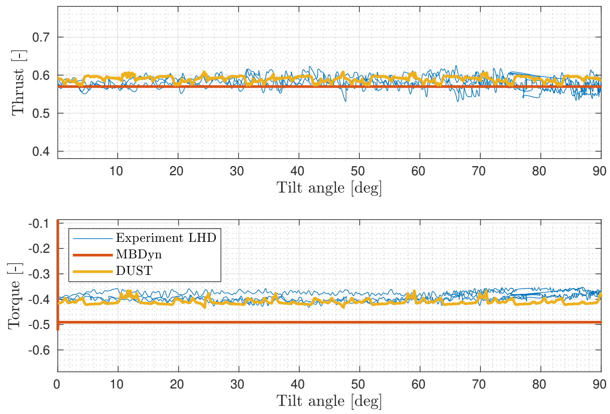


**Figure 12. Thrust and torque for $V_\infty$ = 0 m/s and Ω = 100% RPM.**

2. The experimental results exhibit a hysteresis effect during the conversion–reconversion maneuver, likely attributable to propeller wake effects. To confirm this hypothesis, coupled MBDyn–DUST simulations incorporating unsteady wake and interactional aerodynamics are currently in progress.

3. Notably, when the control torque approaches zero or small values, high-frequency oscillations are observed. This behavior is attributed to the tilting mechanism being unloaded, making it more susceptible to small imperfections that can trigger limit cycle oscillations.

Future work will investigate the static and dynamic loads during conversion at different freestream velocities and correlate the results with the numerical model. The long-term objective of this study is to predict the dynamic behavior of the system in the presence of free-play within the mechanism.

Author contact:
Giacomo Lazzaro giacomo.lazzaro@polimi.it
Michele Zilletti michele.zilletti@leonardo.com

## ACKNOWLEDGMENTS

Funded by Unione Europea - Next Generation EU, Missione 4 Componente 1 CUP D43C23002610001.

## REFERENCES

1. N. Polaczyk, E. Trombino, P. Wei, and M. Mitici, “A review of current technology and research in urban on-demand air mobility applications,” *8th Biennial Autonomous VTOL Technical Meeting and 6th Annual Electric VTOL Symposium 2019*, 2019, pp. 333–343.

2. L. Kiesewetter, K. H. Shakib, P. Singh, M. Rahman, B. Khandelwal, S. Kumar, and K. Shah, “A holistic review of the current state of research on aircraft design concepts and consideration for advanced air mobility applications,” *Progress in Aerospace Sciences*, Vol. 142, 2023. DOI: https://doi.org/10.1016/j.paerosci.2023.100949.

3. Zilletti, M., Prederi, D., Costantini, R., Zaccara, M., Ricciardi, M., Morelli, G., and Masarati, P., “Wind Tunnel Test of a Single Electrical Lift Thrust Unit to Assess Static and Dynamic Loads,” *49th European Rotorcraft Forum (ERF 2023)*, 2023.

4. Balatti, D., Zilletti, M., Duina, A., Zaccara, M., Dispenza, A., and Masarati, P., “Wind Tunnel Test of Two Electrical Lift Thrust Units to Assess Static and Dynamic Loads,” *50th European Rotorcraft Forum (ERF 2024)*, 2024.

5. A. Atoll, B. J. B., “Development of eVTOL Aircraft For Urban Air Mobility At Joby Aviation,” *Vertical Flight Society’s 78th Annual Forum Technology Display*, Vol. 1185, 2022.

6. DEPAPE, P., and Bower, G. C., “Systems and methods for controlling rotor tilt for a vertical take-off and landing aircraft,” US Patent 11,691,724, July 4 2023.

7. Masarati, P., Morandini, M., and Mantegazza, P., “An Efficient Formulation for General-Purpose Multibody/Multiphysics Analysis,” *Journal of Computational and Nonlinear Dynamics*, Vol. 9, 2014. DOI: https://doi.org/10.1115/1.4025628.

8. Tugnoli, M., Montagnani, D., Syal, M., Droandi, G., and Zanotti, A., “Mid-fidelity approach to aerodynamic simulations of unconventional VTOL aircraft configurations,” *Aerospace Science and Technology*, Vol. 115, 2021. DOI: https://doi.org/10.1016/j.ast.2021.106804.

9. Chourdakis, G., Davis, K., Rodenberg, B., Schulte, M., Simonis, F., Uekermann, B., Abrams, G., Bungartz, H. J., Cheung Yau, L., Desai, I., Eder, K., Hertrich, R., Lindner, F., Rusch, A., Sashko, D., Schneider, D., Totounferoush, A., Volland, D., Vollmer, P., and Koseomur, O. Z., “preCICE v2: A sustainable and user-friendly coupling library,” *Open Research Europe*, Vol. 2, (51), 2022. DOI: 10.12688/openresearch europe.14445.2.

10. Savino, A., Cocco, A., Zanotti, A., Tugnoli, M., Masarati, P., and Muscarello, V., “Coupling mid-fidelity aerodynamics and multibody dynamics for the aeroelastic analysis of rotary-wing vehicles,” *Energies*, Vol. 14, 2021. DOI: https://doi.org/10.3390/en14216979.